https://doi.org/10.5194/egusphere-2024-1525
Preprint. Discussion started: 31 May 2024

A new glacier thickness and bed map for Svalbard

Ward van Pelt[1] and Thomas Frank[1]
[1]Department of Earth Sciences, Uppsala University, Sweden
Correspondence: Ward van Pelt (ward.van.pelt@geo.uu.se)

Abstract. Knowledge of the thickness, volume and sub-glacial topography of glaciers is crucial for a range of glaciological, hydrological and societal issues, including, e.g., studies on climate-warming induced glacier retreat and associated sea-level rise. This is not the least true for Svalbard, one of the fastest-warming places in the world. Here, we present a new map of ice thickness and sub-glacial topography for every glacier on Svalbard. Using remotely-sensed observations of surface height, ice velocity, rate of surface elevation change, and glacier boundaries in combination with a modeled mass balance product, we apply an inverse method that leverages state-of-the-art ice flow models to obtain the shape of the glacier bed. Specifically, we model large glaciers with the Parallel Ice Sheet Model (PISM) at 500 m resolution, while we resolve smaller mountain glaciers at 100 m resolution using the physics-informed deep learning-based Instructed Glacier Model (IGM). Actively surging glaciers are modeled using a perfect-plasticity model. We find a total glacier volume (excluding Kvitøya) of 6,800 km$\pm$238 km^3, and a mean ice thickness of 205$\pm$7 m. Validation against thickness observations shows high statistical agreement, and combining the three methods is found to reduce uncertainties. We discuss remaining sources of errors, differences to previous ice thickness maps of the region, and future applications of our results.

1 Introduction

Glaciers outside the Greenland and Antarctic ice sheets currently account for about half of the total land-ice contribution to sea level rise (Hugonnet et al., 2021). About 7% of the total glacier contribution to sea level rise between 1961/62 and 2015/16 came from glaciers in Svalbard and Jan Mayen, with an estimated 687 Gt of glacier mass loss (IPCC, 2023). Svalbard is experiencing among the fastest warming on the planet, as it experiences the direct impacts of amplified warming (Arctic Amplification) following the ongoing retreat of sea ice and associated radiation feedbacks (e.g. Serreze and Barry, 2011; Bintanja and Van der Linden, 2013; Cao et al., 2017). In response to a strong warming trend and weak precipitation increase, Svalbard glaciers have lost mass at a rate of 7$\pm$4 Gt a^{-1} during 2000-2019 due to surface-atmosphere interactions, as expressed by the climatic mass balance (CMB), on top of frontal ablation losses of 2$\pm$7 Gt a^{-1} (Schuler et al., 2020). CMB predictions indicate mass loss acceleration with average CMB values below -50 Gt a^{-1} in 2060 for future emission scenarios RCP4.5 and RCP8.5 (Van Pelt et al., 2021). Based on historical data, structure-from-motion photogrammetry and a space-for-time substitution, Geyman et al. (2022) estimated a doubling of glacier mass loss from 1936-2010 to 2010-2100 with average thinning of -0.67 to -0.92 m yr^{-1} in the latter period.

https://doi.org/10.5194/egusphere-2024-1525
Preprint. Discussion started: 31 May 2024

Knowledge of ice thickness and subglacial topography is relevant for many applications. Mean ice thickness and glacier volume provide estimates of fresh water storage on land. Glacier volume trends directly affect sea level rise (SLR), but also have an impact on future fresh water availability and management. Knowing the ice-free topography after glacier retreat gives insight in future landscape and coastlines, which is relevant for future marine, terrestrial, hydrological, ecosystem and climate modelling studies. A necessity for simulating long-term glacier evolution is detailed knowledge of basal topography under the ice. Whereas a wealth of observational data of surface processes is available, the inaccessibility of the glacier bed complicates direct observations of subglacial topography. To measure distributed fields of basal topography using ground-penetrating radar (GPR) is a laborious and expensive task. As a result, thickness observations exist for only 1-2 % of all glaciers worldwide (Gärtner-Roer et al., 2014; GlaThiDa Consortium, 2020).

Ice flow models simulate ice motion and changing ice geometry and are the common tool to study glacier mass and volume change in past, present and future climates (e.g. Goelzer et al., 2017; Rounce et al., 2023). A major source of uncertainty in glacier modelling, contributing to errors in sea level rise predictions, stems from difficulties in setting initial conditions in the present day that are needed as a starting point for forecasting runs. Knowledge of bed topography and friction is essential for accurate simulation of ice motion and thickening/thinning, but direct observations are scarce (Morlighem, 2022). This has stimulated the development of inverse methods to indirectly estimate the ice thickness distribution from much more abundant surface data, including surface height, mass balance and/or velocity. A range of inverse methods exist to produce ice thickness maps and have been compared in (Farinotti et al., 2017, 2021). Participating approaches ranged from point-based methods (e.g. Linsbauer et al., 2009) to fully-distributed methods (e.g. Van Pelt et al., 2013), and differed regarding the required input datasets (such as mass balance, velocity and surface height change), as well as the ice flow physics used.

The inverse methods used in this study are based on the iterative approach in Frank et al. (2023), which is inspired by the method in Van Pelt et al. (2013) and performs short forward simulations with an ice flow model around the time of collection of observational datasets of distributed velocity, surface height and its change, and mass balance. After every forward simulation (iteration) bed heights are adjusted to reduce mismatches of surface height change. On fast-flowing tide-water glaciers, basal friction is additionally optimized to reduce mismatches with surface velocity data. Using surface height and velocity errors to correct basal conditions has proven to be a fast method to converge to bed height and friction fields that, for the assumed ice flow physics, generate a glacier dynamic state that is consistent with observations (Frank et al., 2023). Uncertainties in observational datasets and model physics introduce errors in the bed, and to prevent "over-fitting" regularization is required, e.g. by smoothing input datasets. The inverse method itself does not introduce errors; in the hypothetical case of a perfect ice flow model and noise-free input datasets, the reconstructed basal conditions would approach reality (there is however a physical limit to the spatial detail that can be resolved as small-scale bed features do not yield any surface expression (Gudmundsson and Raymond, 2008)). Advantages of the method in Frank et al. (2023) are that it can be used with any ice flow model and that the final state at the end of the inversion is a useful initial (spin-up) state for prognostic simulations, as the geometry and dynamics are consistent with surface observations.

In this study, different ice flow models are used to invert for bed topography of small land-terminating glaciers and to invert for bed topography and basal friction on large land-terminating and fast-flowing marine-terminating glaciers. For modelling

https://doi.org/10.5194/egusphere-2024-1525
Preprint. Discussion started: 31 May 2024

large land-terminating glaciers and tide-water glaciers on a 500-m resolution grid, a similar method as in Frank et al. (2023) is used, which employs the ice flow model Parallel Ice Sheet Model (PISM; www.pism.io; Bueler and Brown, 2009) that combines the shallow ice approximation (SIA) and shallow shelf approximation (SSA) to simulate internal deformation and sliding motion respectively. For modelling small land-terminating glaciers, we adopt the same approach as in a recent study by Frank and Van Pelt (2024), where the inverse method was applied to all glaciers in Norway and Sweden, using the machine-learning based Instructed Glacier Model (IGM; Jouvet and Cordonnier, 2023; Cook et al., 2023) as an ice flow model. The advantages of IGM over using traditional (shallow) ice flow models are 1) the ability to use a higher-order physics, which is particularly relevant for mountain glaciers, and 2) severely reduced numerical cost which enables simulations with high spatial resolution. In this study, IGM is used to model small land-terminating glaciers in Svalbard at a 100-m spatial resolution.

Svalbard is home to 1,567 glaciers (1,544 glaciers excluding Kvitøya) with a total area of 33,775 km^2 in ∼2010 (Nuth et al., 2013). Of these glaciers, 186 (12%) are classified as tidewater glaciers, covering an area of 23,986 km^2, equivalent to 71% of the total glacier area (RGI Consortium, 2017, Randolph Glacier Inventory version 6;). 103 glaciers in Svalbard have been reported to surge, and another 103 and 37 are respectively possibly or probably of surge-type (Sevestre and Benn, 2015). Several studies have previously quantified Svalbard's glacier volume and thickness using a wide range of methods. Volume-area scaling methods, often applied in global studies, have given volume estimates ranging from 4,000 km^3 (Ohmura, 2004) to 10,260 km^3 (Radić and Hock, 2010), and various estimates between these extremes (e.g. Hagen, 1993; Grinsted, 2013; Radić and Hock, 2013; Martín-Español et al., 2015). More recently, inverse methods have been used to reconstruct distributed ice thickness in global assessments (Farinotti et al., 2019; Millan et al., 2022) as well as in a dedicated regional study on Svalbard (Fürst et al., 2018). Whereas Farinotti et al. (2019) presented a weighted average thickness distribution based on a set of thickness products produced using different methods, Millan et al. (2022) instead estimated thickness distribution using global high-resolution velocity data and assuming SIA-based ice flow physics and a Weertman sliding law. Millan et al. (2022) estimated Svalbard's glacier volume at 6,855 km^3 (excluding Kvitøya). Fürst et al. (2018) used a two-step mass conservation method (Fürst et al., 2017) that locally calibrates ice viscosity using thickness observations in the Glacier Thickness Database (GlaThiDa; GlaThiDa Consortium, 2020). The method by Fürst et al. (2018) hence locally assimilates the thickness data, and errors were shown to increase with distance to observation locations. Fürst et al. (2018) found a volume estimate of 6,199 km^3, and a likely range of 5,200-7,300 km^3. The thickness results for Svalbard in Farinotti et al. (2019) are a copy of the results in Fürst et al. (2018). Based on this, we only compare our results to the recent thickness datasets presented in Fürst et al. (2018) and Millan et al. (2022).

We present a new thickness and bed height dataset for all glaciers in Svalbard, using a combination of inverse model results using IGM on small land-terminating glaciers (at 100-m resolution) and PISM on large land-terminating and tidewater glaciers (at 500-m resolution). Surging glaciers were modelled separately with a perfect-plasticity method instead, as timing mismatches between the input datasets (e.g. DEM from 2010 and velocity map from 2017-2018) did not allow for accurate inversion of these glaciers using the Frank et al. (2023) method. In the following sections, we describe the input data (Section 2), introduce the inverse method (Section 3), present the bed and thickness maps and compare them against existing products (Section 4), discuss uncertainties (Section 5), and present conclusions (Section 6).

https://doi.org/10.5194/egusphere-2024-1525
Preprint. Discussion started: 31 May 2024

Table 1. Overview of the datasets used in the inverse method.

Variable	Method/database	Orig. resolution	Time-frame	Source
Digital elevation model	Aerial photos	20 m	2009-2012	Norwegian Polar Institute (2014)
Surface height change	ASTER & ArcticDEM	100 m	2010-2019	Hugonnet et al. (2021)
Ice velocity	Landsat 8, Sentinel-2 & Sentinel-1	50 m	2017-2018	Millan et al. (2022)
Climatic mass balance	Energy balance - firn model (EBFM)	1,000 m	2010-2019	Van Pelt et al. (2019)
Ice thickness	Glacier Thickness Database (GlaThiDa)	966,408 data points	1983-2016	GlaThiDa Consortium (2020)
Frontal ablation	GlaThiDa & ITS_LIVE	Estimate per glacier	2010-2020	Kochtitzky et al. (2022)
Glacier outlines	Randolph Glacier Inventory 6.0	-	2007-2008	RGI Consortium (2017)

2 Data

Various remote sensing and model-based datasets of surface conditions are used as "input" in the inverse method, including distributed maps of surface elevation, climatic mass balance, surface height change, glacier outlines, surface velocity, and glacier-average frontal ablation. In addition, ice thickness observations are used for calibration and validation. The data is summarized in Table 1. Distributed maps of surface elevation, surface height change, velocity, climatic mass balance, thickness observations, and glacier outlines are shown in Fig. 1. For more details about the input datasets, the reader is referred to the data sources in Table 1.

3 Methods

Three different approaches are used to generate thickness and bed maps for all glaciers in Svalbard. We split Svalbard's glaciers into three groups (see also Fig. 1c): 1) all glaciers that are smaller than 100 km^2 and not of tide-water and surge-type (Sevestre and Benn, 2015), 2) all glaciers that are larger than 100 km^2 and those smaller than 100 km^2 that were of tide-water or surge-type, but not surging during 2017-2018 (Koch et al., 2023), 3) all glaciers that were reported to surge during 2017-2018. Glaciers in 1) are modeled using the Instructed Glacier Model (IGM; Jouvet and Cordonnier, 2023) as in Frank and Van Pelt (2024) (Sect. 3.2). Glaciers in 2) are modeled using the Parallel Ice Sheet Model (PISM; Bueler and Brown, 2009) as in Frank et al. (2023) (Sect. 3.1). Finally, ice thickness for glaciers in 3) is estimated using the perfect-plasticity assumption (Nye, 1952). The rationale behind the grouping is that glaciers in group 1) can be modeled with higher resolution, higher-order physics, and low computational cost using the machine-learning model IGM. Large tide-water glaciers and ice caps, combining slow internally deforming sections with fast-flowing areas, are effectively modeled with PISM (Bueler and Brown, 2009). A simpler perfect-plasticity approach is needed for the surging glaciers in 3), as mismatches in time-frames of input datasets (most prominently DEM, surface velocity & surface height change) would induce major errors when applying iterative inverse

https://doi.org/10.5194/egusphere-2024-1525
Preprint. Discussion started: 31 May 2024

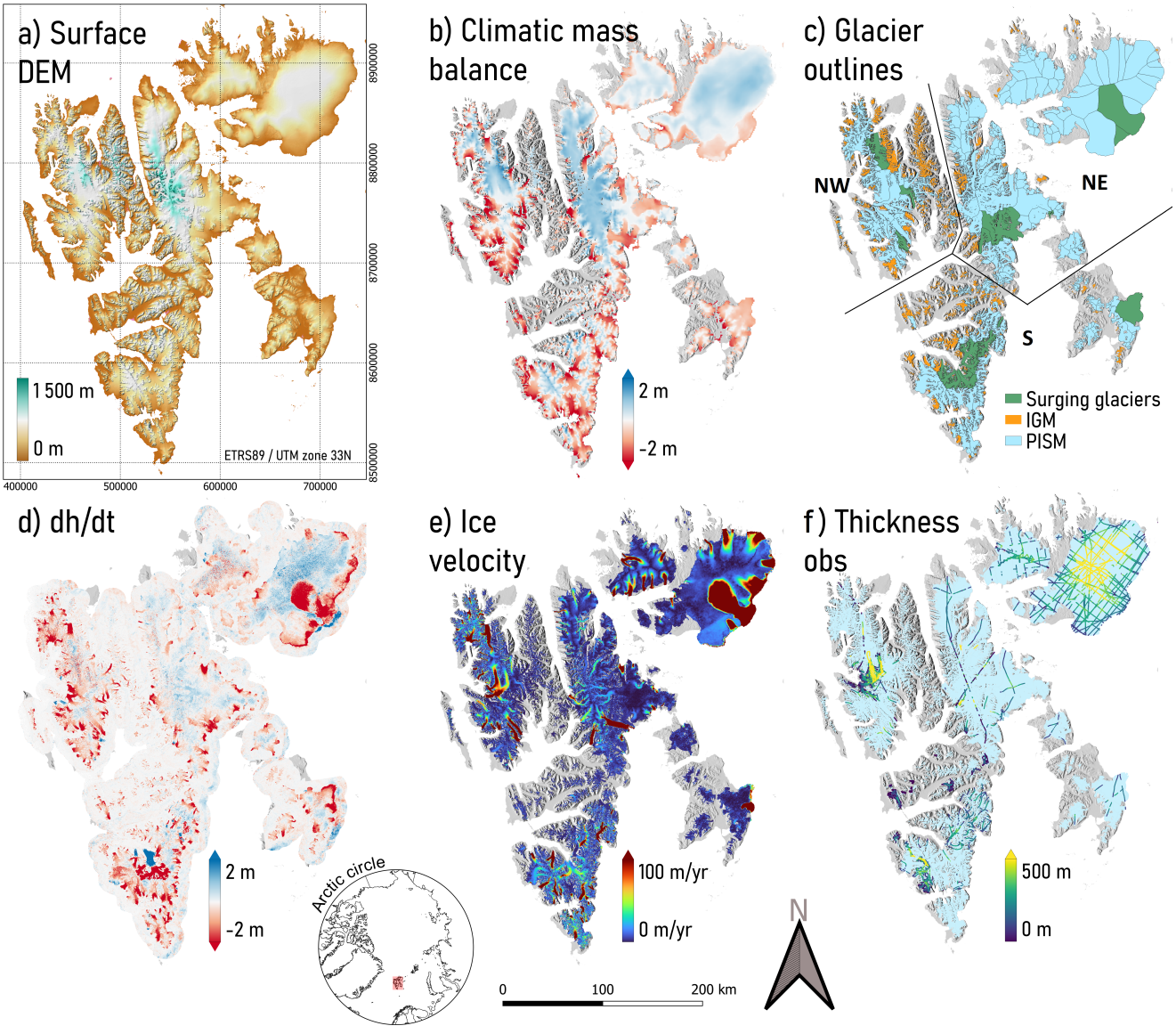

Figure 1. Overview maps of the input data sets used in the inverse modeling. Data sources and information are given in Table 1. The regions northwest (NW), northeast (NE) and southern Svalbard (S) are marked in c.

methods. One nuance to the three groups above is that all glaciers that are part of / connected to larger ice caps are modeled with the same model (PISM), to avoid thickness jumps at the ice divides. The three methods are described in more detail below.

https://doi.org/10.5194/egusphere-2024-1525
Preprint. Discussion started: 31 May 2024

3.1 Inversion using PISM

In preparation for the inversion, input datasets of the digital elevation model (DEM), surface height change, surface mass balance and velocity were averaged/interpolated from their original grid (20-1,000 m resolution; Tab. 1) to the 500-m grid used by the ice flow model. Similarly, glacier outlines from the RGI were down-sampled onto the 500-m model grid to generate a mask separating glacier and glacier-free terrain.

The ice flow model PISM is used to perform iterative short (0.001 years) forward simulations of ice flow and geometric change for all glaciers in group 2), i.e. large (>100 km^2) glaciers and small quiescent surge-type glaciers. As in Frank et al. (2023), PISM uses the combined shallow-ice, shallow-shelf approximation (Bueler and Brown, 2009) to model both ice flow by internal deformation and sliding, the latter being described by a linear sliding law with spatially varying yield stress τ_c. A flow enhancement factor for the SIA (SIA_e) is used, set here to 3 as in previous applications of PISM in Antarctica (Martin et al., 2011), Greenland (Bochow et al., 2023) and Iceland (Robinson, 2018). Ice temperature, and with that ice softness (3.1689e-24 Pa^{-3} s^{-1}), are assumed to be constant, i.e. thermodynamics are not modeled. After every 0.001-year model run, modeled and observed surface height change ($\frac{dh_{\text{mod}}}{dt}$ and $\frac{dh_{\text{obs}}}{dt}$) are compared to calculate a misfit that is used to locally adjust the bed height b before the next model run:

$$b_{\text{new}} = b_{\text{old}} - \beta \left(\frac{dh_{\text{mod}}}{dt} - \frac{dh_{\text{obs}}}{dt} \right) \tag{1}$$

where β is a coefficient, set here to 0.25. Following Frank et al. (2023) we apply a simultaneous correction of the surface height, yet of opposite sign and a magnitude that is θ times the bed height misfit. The surface adjustments were previously found to stabilize the inversion in places where the ice flow model is not well able to simulate observed flow patterns e.g. because of simplifying assumptions in the stress balance equations (Frank et al., 2023). Similar to Frank et al. (2023) we update basal friction (by modifying the yield stress τ_c). The initial friction field is estimated using $\tau_c = \left| \frac{\tau_d}{u_{\text{obs}}} \right|$, where τ_d is the driving stress and u_{obs} is the observed ice velocity. Based on test runs, we found the best performance (lowest thickness errors) when updating τ_c only once after 400 model iterations. The inverse experiment uses a total of 800 iterations (bed height corrections). The initial bed at the start of the first model iteration b_{init} is set to a bed that is estimated using the perfect-plasticity assumption (Nye, 1952; Li et al., 2012):

$$b_{\text{init}} = h - \frac{\tau}{\rho g \sin \alpha}, \tag{2}$$

where h is the surface height, τ is a yield constant, ρ is the ice density (900 kg m^{-3}), g is the gravitational acceleration (9.8 m s^{-2}) and α is the absolute surface slope. For surface slopes smaller than α_{min}, $\alpha = \alpha_{\text{min}}$, which is needed to avoid excessively large thickness values for low-sloping areas. Parameter values for α_{min} and τ were estimated based on calibration against thickness observations on surging glaciers, as described further in Sect. 3.3 below.

As in Frank et al. (2023), climatic mass balance per glacier is re-projected using a regression-based linear function of climatic mass balance with elevation. Similarly, we re-project surface height change using linear fitting against elevation. The linear regressions were previously found to increase the accuracy of reconstructed ice thicknesses as erroneous local spatial variations in the surface height change and velocity datasets no longer affect the thickness reconstruction (Frank and Van Pelt, 2024).

https://doi.org/10.5194/egusphere-2024-1525
Preprint. Discussion started: 31 May 2024

Differencing of the climatic mass balance and surface height change results in the apparent mass balance (Farinotti et al., 2009), which is forced to sum to zero for every land-terminating glacier by applying spatially constant bias corrections per glacier. For tide-water glaciers, instead the glacier-summed apparent mass balance minus frontal ablation (Tab. 1; Kochtitzky et al., 2022) is enforced to equal zero. The above corrections assure mass conservation for every glacier, although compensating errors may occur, e.g. in the case of erroneous frontal ablation estimates resulting in a bias of the apparent mass balance. Despite the above measures to conserve mass, modeled glaciers often tend to become too thin at their fronts due to mass 'escaping' through the lateral boundaries set by the RGI outlines (Frank and Van Pelt, 2024). To compensate for this mass loss, we apply a fixed correction for all glaciers equal to M_{corr}.

Frank et al. (2023) applied post-processing of thicknesses when modeled velocities in zones dominated by slow internal deformation flow were higher than observed even for $\tau_c \rightarrow \infty$. A different approach is applied here based on the logic that in zones where flow is controlled by internal deformation, the yield stress is an irrelevant parameter. We therefore introduced an observed velocity threshold $u_{\text{thres}} = 25$ m yr^{-1} to identify regions where slow flow prevailed and no friction updates were applied.

Frank and Van Pelt (2024) previously found that ice thickness estimates improved by applying surface updates and mass balance corrections. With this in mind, we calibrated θ and M_{corr}, by searching for a minimum mean absolute error between modeled and observed (GlaThiDa) ice thicknesses for all observed locations in Svalbard. Optimum values of $\theta = 0.4$ and $M_{\text{corr}} = 0.4$ m w.e. yr^{-1} were found, yielding a mean absolute error (MAE) of 58.1 m. More statistics on the comparison with observations are given in Sect. 4.2. These statistics are after post-processing of thicknesses using a moving-average smoothing filter a with window size of 3 cells. This was found to give a reduction of the mean absolute error (-2.2 m), and an increase of Pearson correlation (+0.014), relative to non-post-processed thicknesses. Bed heights are calculated by subtracting thicknesses from the DEM.

Sensitivity tests were performed with a perturbed initial bed (zero ice thickness), magnitude of surface updates ($\theta = 0.2$ and $\theta = 0.8$), and mass balance correction ($M_{\text{corr}} = 0.2$ m w.e. yr^{-1} and $M_{\text{corr}} = 0.6$ m w.e. yr^{-1}). Results are visualized in Figure 2. Figure 2 shows that M_{corr} perturbation mostly affects lower elevation areas, whereas θ adjustments mainly impact slow-flowing high-elevation areas; this supports the choice of these two parameters for calibration. Impacts of perturbing M_{corr} are increases of the MAE relative to the thickness observations of 1.3 m ($M_{\text{corr}} = 0.2$ m w.e. yr^{-1}) and 0.3 m ($M_{\text{corr}} = 0.6$ m w.e. yr^{-1}); perturbing θ yielded increases of the MAE of 2.5 m ($\theta = 0.2$) and 0.2 m ($\theta = 0.8$). Furthermore, perturbing M_{corr} and θ introduce biases of the mean thickness of -10.6 (M_{corr} =0.2 m w.e. yr^{-1}), 7.3 (M_{corr} =0.6 m w.e. yr^{-1}), 5.1 ($\theta = 0.2$), and -10.8 m ($\theta = 0.8$). The extreme case to start with no ice results in a weaker performance (e.g. 12.0 m increase in MAE), highlighting the importance of starting with a reasonable first guess of the bed topography. It is noteworthy that all perturbation experiments give a final bed at the end of the inversion that has a lower MAE than the initial (unperturbed) perfect-plasticity bed, which has an MAE equal to 77.5 m (compared with 58.1 m for our best run).

https://doi.org/10.5194/egusphere-2024-1525
Preprint. Discussion started: 31 May 2024

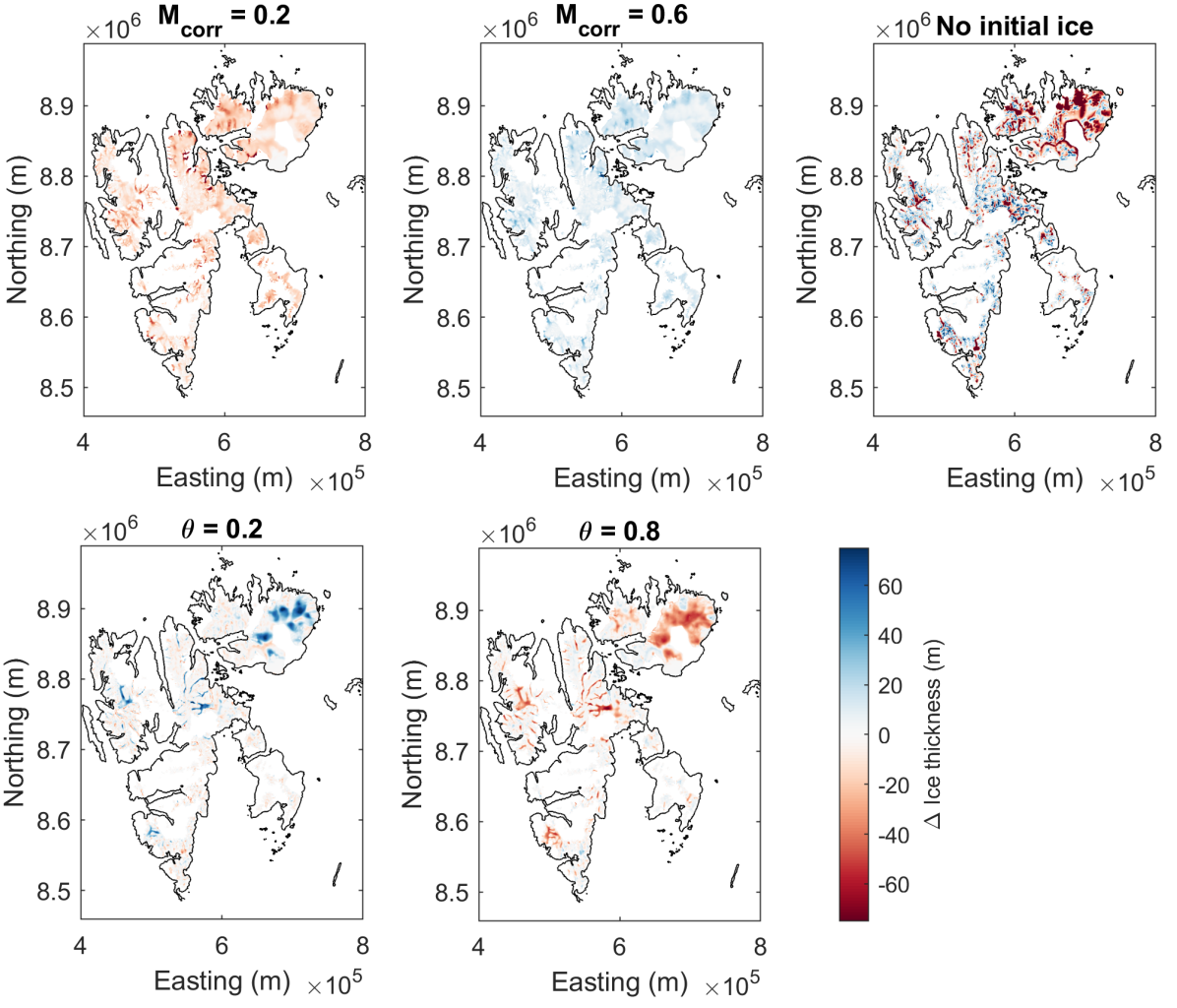

Figure 2. Sensitivity of PISM-modelled ice thickness for perturbed M_{corr}, θ and initial bed. Thickness differences are calculated by subtracting the thickness of the reference run from the thickness of the perturbation experiment.

3.2 Inversion using IGM

The inversion for glaciers from group 1 follows a largely congruent workflow with the one above in that the principle is based on Frank et al. (2023) where bed updates (eq.(1)) and surface updates are executed iteratively. The main differences are the ice flow model (IGM v2.0.4 instead of PISM) and a few parameter and processing choices. The method is closely aligned with Frank and Van Pelt (2024).

https://doi.org/10.5194/egusphere-2024-1525
Preprint. Discussion started: 31 May 2024

The spatial resolution is 100 m which the DEM and glacier outlines are down-sampled to. The DEM is furthermore smoothed in the ablation area with a two-sigma Gaussian filter; this strategy was found to be superior to not smoothing or to smoothing over the entire glacier area. The climatic mass balance for each glacier is downscaled from the original 1000 m resolution to 100 m by fitting an elevation dependent piece-wise linear function with two segments and a breakpoint at the ELA to the mass balance product by Van Pelt et al. (2019) of a given glacier and glaciers within a buffer of 10 km. Taking neighboring glaciers into consideration is done to avoid poorly-constrained fits for small glaciers as a result of the coarse resolution of the original product. The apparent mass balance is calculated as above based on this new climatic mass balance and dh/dt.

IGM (Jouvet and Cordonnier, 2023) is a physics-informed deep learning model that emulates higher-order ice flow while being computationally efficient. The underlying architecture is a Convolutional Neural Network (CNN) which is retrained as the model runs. This is achieved by comparing the solution of the CNN to that of an actual higher-order solver and updating the CNN weights based on that mismatch every 10th model iteration, ensuring a close alignment between the CNN and process model solutions. IGM includes a Weertman-type sliding law with a sliding coefficient c and it allows to set the ice viscosity parameter A. Calibration is done by finding one global value for A and c which minimizes the mean error to ice thickness observations. By not allowing A to exceed A_{max} =78 MPa^{-3}a^{-1} (the value corresponding to an ice temperature of 0°C) and enforcing c=c_{min}=100 km MPa^{-3}a^{-1} if A<A_{max} (following a simplifying assumption that no basal sliding occurs for cold ice as in Jouvet (2022) and Frank and Van Pelt (2024)), the calibration procedure yields the optimal parameters $A = 78$ MPa^{-3}a^{-1}, $c = 8000$ km MPa^{-3}a^{-1}. These values are applied uniformly to all glaciers in group 1.

The initial thickness field is obtained using a perfect plasticity approach (eq. (2)) with $\tau = 100$ kPA and α_{min}= 0.04. Then, using IGM, 5000 model years are simulated during which bed (with β=1) and surface updates (with θ=0.15) are applied. In contrast to the PISM approach, basal friction is not updated but kept fixed. This follows from the assumption that there are smaller spatial variations in the basal friction fields of small mountain glaciers compared to large (tidewater) glaciers, meaning that one initial calibration of the spatially uniform c is sufficient. To account for mass escaping through the lateral glacier boundaries a different strategy than in the PISM approach is pursued, as in Frank and Van Pelt (2024). Specifically, after 3000 model years and for each glacier individually, the integrated apparent mass balance of those areas within the glacier mask that are ice free (which is equal to the mass leakage rate) divided by the total glacier area is added to the specific apparent mass balance. Doing so, the mass leaking out on the lateral glacier boundaries is fed back to the glacier via a correction of the apparent mass balance. The final thickness field is obtained by interpolating gaps in the modelled thicknesses and applying a thickness-dependent Gaussian filter as in Frank and Van Pelt (2024).

3.3 Surging glaciers

Thickness estimation using iterative inverse methods as in Sect. 3.1 and 3.2 ideally uses input datasets of surface height, surface height change, velocity, mass balance and frontal ablation that represent the same point in time. In practice, accessible datasets will have different time-frames, introducing a source of error for inverse estimated thicknesses. Such errors are small for glaciers that are near steady-state or undergoing gradual change. Conversely, errors become considerable for glaciers that are undergoing rapid dynamic changes, e.g. in the event of surge initiation. In the latter case, a simpler method depending on fewer

https://doi.org/10.5194/egusphere-2024-1525
Preprint. Discussion started: 31 May 2024

input datasets is desirable. Here, we apply the perfect-plasticity assumption to estimate thicknesses for 13 glaciers, including e.g. Basin-3, Negribreen and Tunabreen, that actively surged during 2017-2018 (equivalent to the time-frame for the velocity dataset), as identified by Koch et al. (2023). The application of the perfect-plasticity assumption is the same as when generating the initial bed in the PISM-based inversion (Sect. 3.1). To find optimum values of minimum slope α_{min} and yield constant τ all combinations with $\alpha_{\text{min}} = 0.010 : 0.001 : 0.040$ and $\tau = 0 : 2 : 100$ kPa were tested to find an optimum combination (lowest RMSE for all available thickness data on the 13 actively surging glaciers). This resulted in $\alpha_{\text{min}} = 0.014$ and $\tau = 52$ kPa.

3.4 Combining the thickness datasets

The three inverse approaches (Sect. 3.1-3.3) generate distributed thickness and bed height datasets at different spatial resolutions: 100-m for the IGM-modelled glaciers and 500-m for both the PISM-modelled and the surging glaciers. To create a uniform combined map of ice thickness (and basal topography), results for the PISM-modelled and surging glaciers on the 500-m resolution grid have been re-projected to the finer 100-m resolution grid used by IGM using nearest-neighbor interpolation. Finally, to improve spatial detail of the outlines of the PISM-modelled and surging glaciers, glacier extent has been clipped to a 100-m resolution glacier mask extracted from the RGI dataset (RGI Consortium, 2017).

3.5 Estimating volume uncertainty

Given model complexity analytical error propagation of modelling errors is not feasible to estimate the uncertainty of the calculated ice volume for all glaciers. We instead adopt an alternative statistical method. The total volume V of all glaciers is:

$$V = \bar{H} A, \tag{3}$$

where $\bar{H}$ is the mean ice thickness and A is the area. Standard error propagation then implies that the standard error σ_V results from errors in $\bar{H}$ and A as follows:

$$\sigma_V = V \sqrt{\left(\frac{\sigma_A}{A}\right)^2 + \left(\frac{\sigma_{\bar{H}}}{\bar{H}}\right)^2}. \tag{4}$$

The term $\frac{\sigma_A}{A}$ is the relative area error resulting from uncertainty of outlines. Nuth et al. (2013) previously estimated this uncertainty 0.01-0.02 (1-2 %) for glaciers in Svalbard; we therefore assume an uncertainty of $\frac{\sigma_A}{A}$ =0.015 applies here. The term $\frac{\sigma_{\bar{H}}}{\bar{H}}$ is the relative mean thickness error. Through calibration of our inverse method, we effectively removed the bias between the average modeled and observed thickness, implying a negligible mean thickness error for the observed glaciers. This does not mean that average modeled thicknesses are bias-free at the Svalbard-wide scale, because of the smaller sample size of the observed glaciers relative to the total number of glaciers. In other words, a volume error may result from the fact that we calibrate against a finite sample of thickness data and use the same model setup also for glaciers without observations. To calculate $\sigma_{\bar{H}}$ we first calculate individual biases for all of the 169 glaciers in Svalbard with thickness observations in at least 10 model grid cells (on the 100x100 m grid), which gives values ranging from -154 to 163 m, and a distribution of biases that is normally distributed according to a Lilliefors test. In the next step, we calculate the standard deviation of the 169 biases,

https://doi.org/10.5194/egusphere-2024-1525
Preprint. Discussion started: 31 May 2024

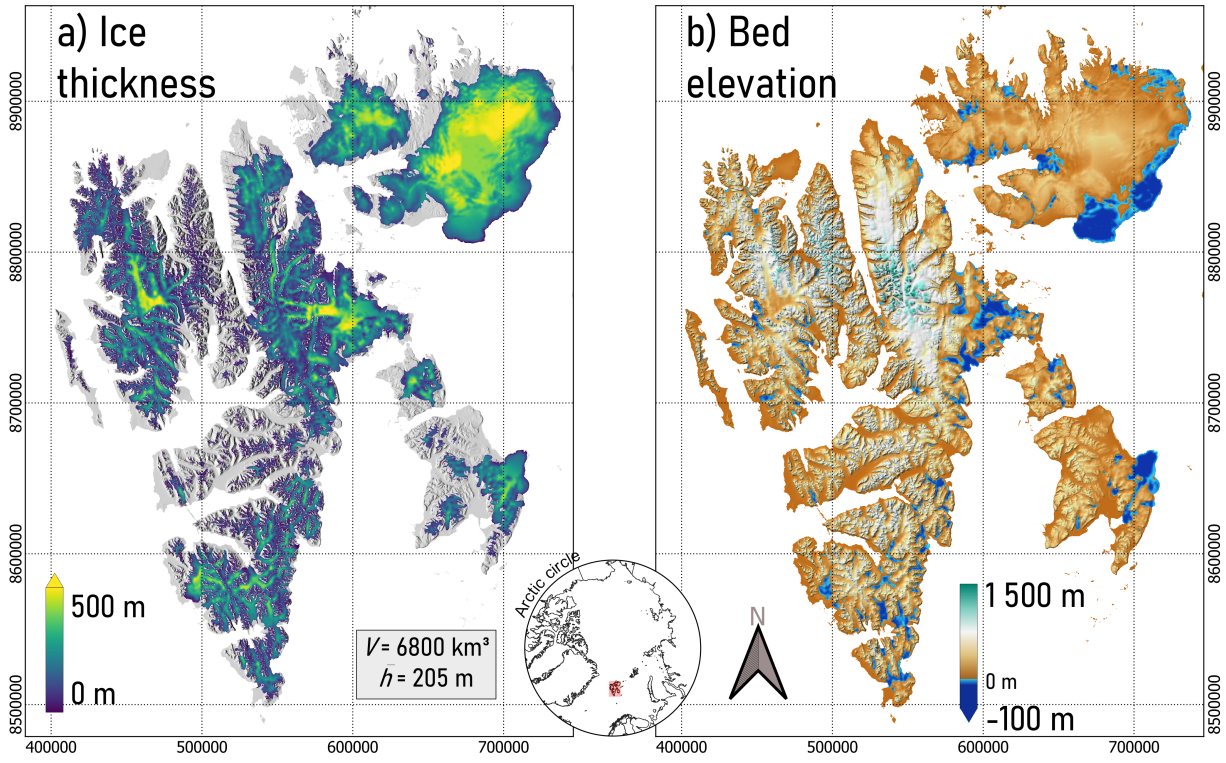

Figure 3. Ice thickness and basal topography for all glaciers in Svalbard (excluding Kvitøya).

giving 45.6 m, implying that if we calibrated against data from only one glacier, the mean modeled thickness would be off by between -45.6 and $+45.6$ m with a likelihood of 68 %. Since we did not use one, but instead 169 glaciers for calibration, the mean thickness error for all observed glaciers $\sigma_{\bar{H}}$ is then calculated by dividing with the square-root of the number of observed glaciers ($\sqrt{169}$), giving $\sigma_{\bar{H}}$ =3.5 m. With a mean observed thickness $\bar{H} = 257.2$ m, the relative thickness error $\frac{\sigma_{\bar{H}}}{\bar{H}}$ then becomes 0.014 (or 1.4%). As a result, we find a (relative) standard error of volume $\frac{\sigma_V}{V}$ of 2.1 % from uncertainties in the area (outlines) and mean thickness; the 90-% confidence interval ($\pm 1.65 \frac{\sigma_V}{V}$) is hence ± 3.5 %.

4 Results & Discussion

4.1 Bed height, ice thickness and volume

Maps of ice thickness and bed topography, combining results from the three methods (Sect. 3), are shown in Figure 3. The mean thickness of all glaciers and ice caps in Svalbard, excluding Kvitøya, is estimated at 205 m. Ice volume equals 6,800 km^3, of which an estimated 315 km^3 (4.6 %) lies below sea level. Total volume uncertainty, with a 90% confidence interval, is

https://doi.org/10.5194/egusphere-2024-1525
Preprint. Discussion started: 31 May 2024

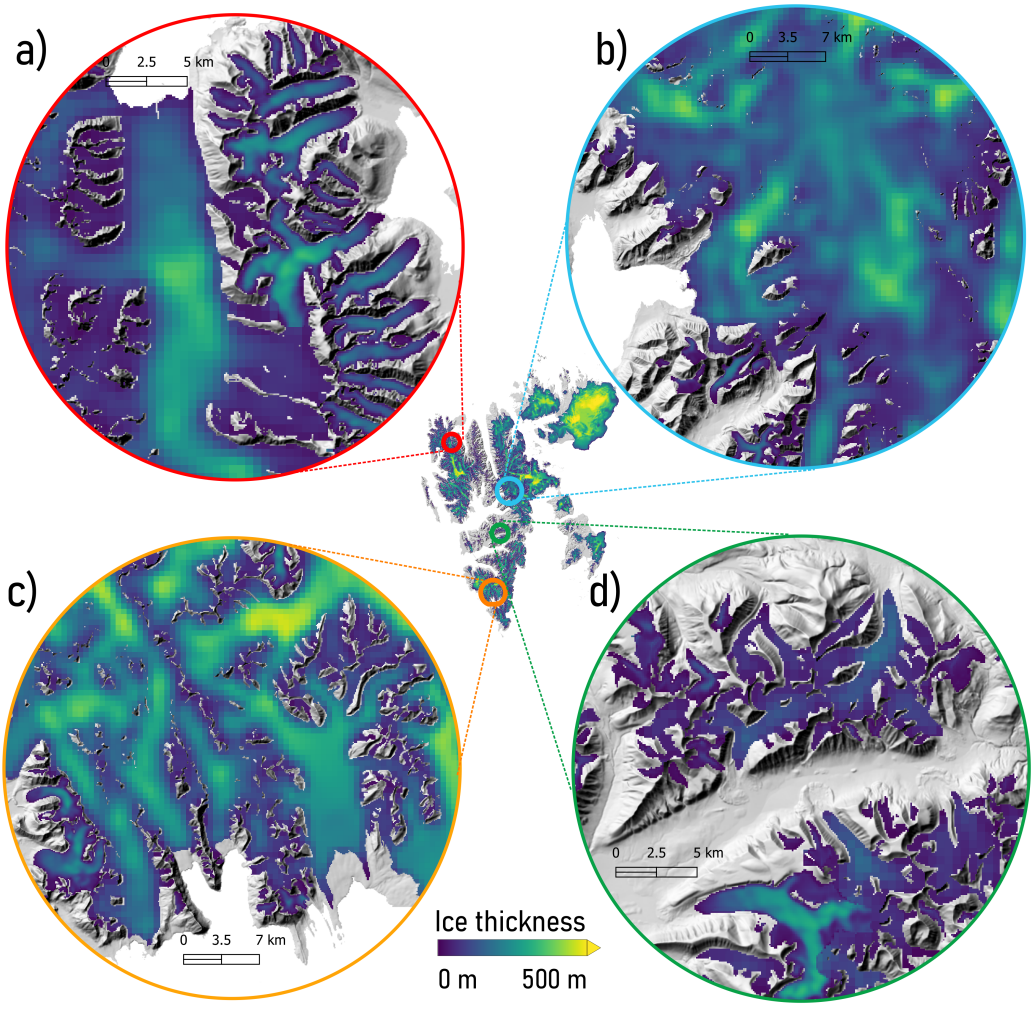

Figure 4. Ice thickness in selected regions in northwest (a), central (b,d), and southern Svalbard (c).

estimated at ± 238 km^3 (± 3.5 %; Sect. 3.5). Assuming an ice density of 917 kg m^{-3}, a seawater density of 1027 kg m^{-3} and a global ocean area of 3.618×10^8 km^2 implies that the Svalbardian glaciers would raise global mean sea level by 16.3 ± 0.6 mm if they melted completely. The largest ice thicknesses are found on Austfonna (Nordaustlandet), Holtedahlfonna (northwest Spitsbergen) and Hinlopenbreen (eastern Spitsbergen). Ice thickness for a selection of four regions (Fig. 4) shows how thickness estimates from IGM and PISM are combined; thickness maps for small land-terminating glaciers contain more spatial detail (100-m resolution) than other glaciers (500-m resolution).

A glacier-averaged thickness comparison for tidewater (TW) and land-terminating (LT) glaciers is shown in Figure 5. The median glacier-average thickness is about four times larger for tide-water glaciers (162 m) than for land-terminating glaciers (42 m). Both land-terminating and tidewater glaciers are on average thickest in northeast Svalbard (LT: 55 m, TW: 183 m) and

https://doi.org/10.5194/egusphere-2024-1525
Preprint. Discussion started: 31 May 2024

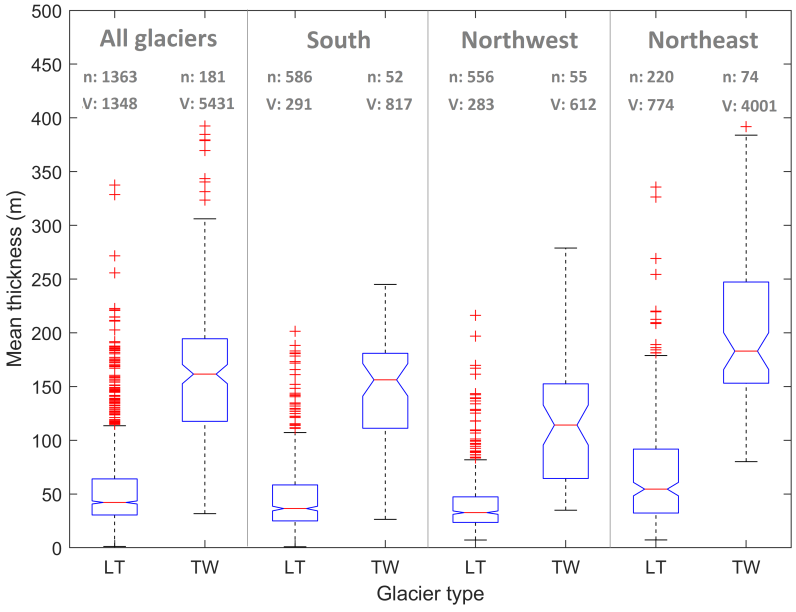

Figure 5. Boxplots showing average glacier thickness for land-terminating (LT) and tide-water (TW) glaciers for all glaciers, and split into southern, northwestern and northeastern glaciers. In each category, n is the number of glaciers and V is total glacier volume (in km^3). Region boundaries for south, northwest and northeast Svalbard are shown in Fig. 1c.

least thick in northwestern Svalbard (LT: 33 m, TW: 114 m). There are 7.5 times more land-terminating glaciers (1,363) than tidewater glaciers (181), however, land-terminating glaciers only comprise 20% (1,348 km^3) of the total glacier volume. Basin-3 on Austfonna is Svalbard's largest glacier, both in terms of area (1,226 km^2) and volume (421 km^3). Etonbreen, Austfonna, is the glacier with the largest average thickness (393 m). Primarily due to the small glacier size, no thicknesses could be estimated for a glacier area of 29 km^2, equivalent to 0.09% of the total glacier area, and, given their below-average thickness, an even smaller fraction of the total glacier volume.

The area and volume distributions with elevation for glaciers in southern, northwestern, and northeastern Svalbard (Fig. 6; regions defined in Fig. 1c), show that the volume and area both peak at surface elevations equivalent to (southern Svalbard) or slightly above the equilibrium line altitude (ELA; northwest and northeast Svalbard) in 1957-2018 (Van Pelt et al., 2019). With an expected rise of the ELA (Van Pelt et al., 2021), strongest in southern Svalbard, the relative size of the accumulation zones to the total glacier area (accumulation area ratio) will drop from 43 to 6 % in southern Svalbard, 58 to 27 % in northwestern Svalbard, and 71 to 41 % in northeastern Svalbard from 1957-2018 to 2019-2060. Similarly, the ice volume with a corresponding surface elevation above the ELA will drop from 35 to 4 % in southern Svalbard, 58 to 24 % in northwestern Svalbard, and 77 to 45 % in northeastern Svalbard. The marked drop in southern Svalbard can in part be ascribed to a pronounced narrow peak in hypsometry at low elevations, as previously discussed in Noël et al. (2020) and Van Pelt et al. (2021). Furthermore, it can be argued that the glacier state, in terms of accumulation area ratio, in northeastern Svalbard in 2019-60 is comparable to the state

https://doi.org/10.5194/egusphere-2024-1525
Preprint. Discussion started: 31 May 2024

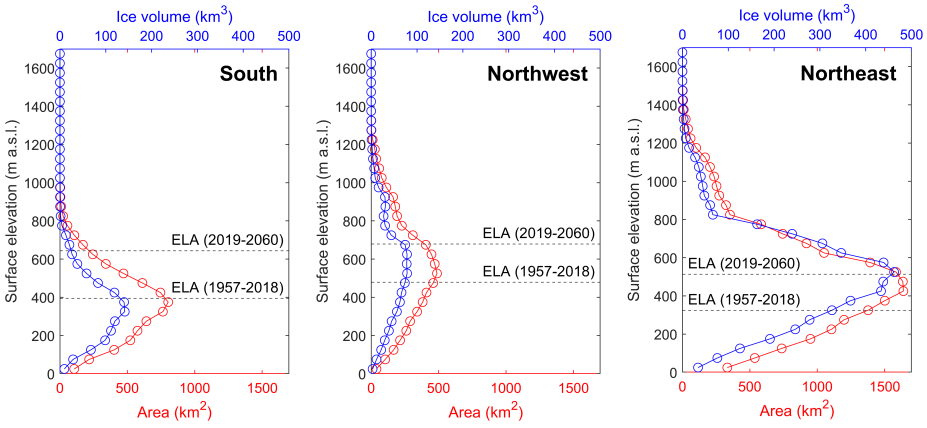

Figure 6. Glacier area (red) and volume in 50-m elevation bins in south (left), northwest (middle) and northeast Svalbard (right). ELA values for 1957-2018 and 2019-60 are taken from Van Pelt et al. (2019, 2021). Region boundaries for south, northwest and northeast Svalbard are shown in Fig. 1c.

Table 2. Comparison of thickness products against point measurements in GlaThiDa.

Thickness dataset	R	MAE (m)	RMSE (m)	Bias (m)
PISM+surging glaciers (500 m)	0.81	57.2	75.5	0.2
IGM glaciers (100 m)	0.77	38.0	50.1	0.1
Millan (PISM+surging glaciers, 500 m)	0.71	81.1	107.2	23.1
Millan (IGM glaciers, 100 m)	0.76	38.1	49.3	-11.4

in southern Svalbard in 1957-2018, i.e. changes in northeastern Svalbard are trailing changes in southern Svalbard by around six decades. Finally, it is noteworthy that the above analysis of area and volume responses to ELA changes disregards the amplifying effects of an associated drop in the surface height as glaciers thin. Hence, the presented reductions in accumulation area ratio and volume above the ELA should be regarded as conservative estimates.

4.2 Comparison with thickness data & other studies

Since the thickness data were only used to optimize spatially independent model parameters, the thickness observation dataset is useful to validate spatial thickness variability. A point-by-point comparison of modeled and observed thickness values is shown in Figure 7. It should be noted that estimated thicknesses are available at two different resolutions (100 m for IGM modeled glaciers, and 500 m for PISM modeled and surging glaciers). It therefore is not feasible to perform a direct comparison for all data at once, as it would involve rescaling (downscaling or averaging) of one of the two datasets to create a dataset with

https://doi.org/10.5194/egusphere-2024-1525
Preprint. Discussion started: 31 May 2024

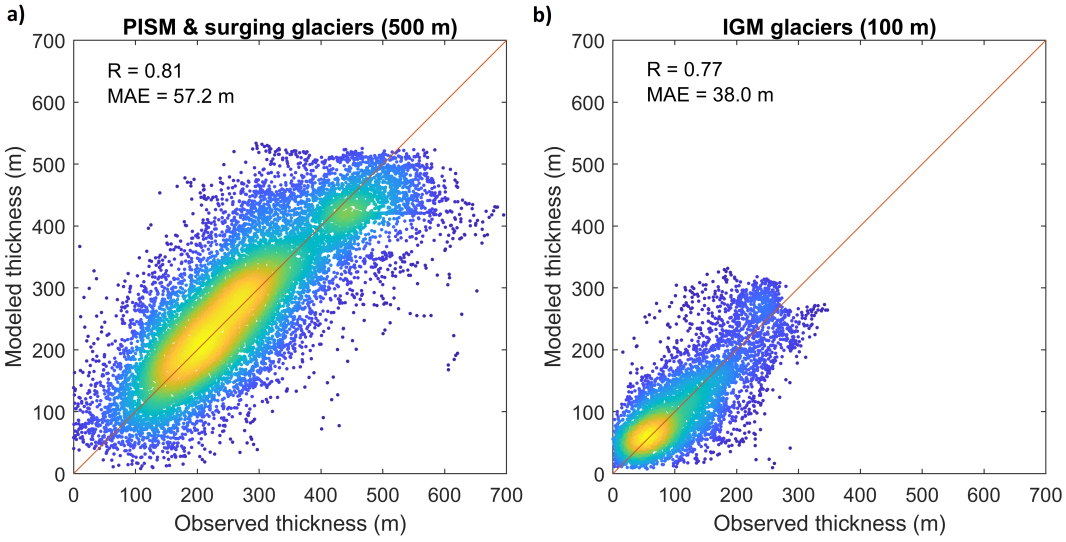

Figure 7. Comparison of modeled and observed ice thickness for glaciers modeled with PISM and surging glaciers(a), and glaciers modeled with IGM (b). Thickness observations are from the GlaThiDa database (GlaThiDa Consortium, 2020). The comparison in a) is based on 500-m resolution output, whereas the comparison in b) is based on 100-m resolution output. The dot color represents the density of data points, ranging from dark blue (lowest density) to bright yellow (highest density).

a constant spatial resolution; the rescaling itself would affect performance metrics of the rescaled data. Based on the above, we instead perform a comparison of estimated and observed thicknesses at two different resolutions, i.e. at 500 m (glaciers modeled with PISM & surging glaciers) and 100 m (glaciers modeled with IGM). Observed thicknesses on the 100 and 500 m grids were estimated by averaging all point observation data falling within every 100 or 500 m grid cell respectively.

For all PISM-modeled and surging glaciers, we find a mean absolute error of 57.2 m, root-mean-square error of 75.5 m and R-correlation of 0.81. This can be compared with a higher RMSE of 107.2 m and lower $R = 0.71$ by Millan et al. (2022) for the same glaciers. For all IGM-modeled glaciers (at 100 m resolution), we find that Millan et al. (2022) produce a similar match with the observations with an MAE of 38.1 m (versus 38.0 m in this study), RMSE of 49.3 m (versus 50.1 m in this study) and $R = 0.76$ (versus $R = 0.77$ in this study). Millan et al. (2022) do experience a considerable negative bias of -11.4 m (versus 0.1 m in this study) for IGM-modeled glaciers and conversely, a strong positive bias (23.1 m) for PISM-modeled and surging glaciers, suggesting an overestimation of thickness for large glaciers and an underestimation for small glaciers. The scatter plots in Fig. 7a-b reveal that the clouds of points are distributed well around the 1:1 line, suggesting no apparent biases for small or large thicknesses. This is an indication that the degree of smoothness/detail in the bed (height of bed peaks and depth of subglacial troughs) is modeled well, e.g. a too-smooth bed would have resulted in an underestimation of large thicknesses and overestimation of small thicknesses. It should be noted that while modeled thicknesses never exceed 560 m, there are some thickness observations indicating ice thicknesses >600 m.

https://doi.org/10.5194/egusphere-2024-1525
Preprint. Discussion started: 31 May 2024

It is noteworthy that in case PISM was used for the glaciers currently modeled with IGM, the MAE would increase to 42.7 m (IGM: 38.0 m), RMSE to 54.1 m (IGM: 50.1 m) and R would drop to 0.71 (IGM: 0.77). The superior performance of IGM for small glaciers is expected, as IGM uses higher-order physics, whereas shallowness assumptions in PISM reduce its performance on small glaciers in variable terrain. We further argue that the combination of SIA and SSA in PISM is well-suited for simulating fast-flowing tidewater glaciers and ice caps. The above highlights the benefit of combining the methods to reduce uncertainties for different types of glaciers.

A spatial comparison of our thickness map with previous maps presented in Millan et al. (2022) and Fürst et al. (2018) is shown in Figure 8. Millan et al. (2022) found a higher volume (6,855 km^3) and average thickness (207 m), while Fürst et al. (2018) found lower volume (5,963 km^3) and mean thickness (182 m) estimates. It should be noted that, in contrast to Millan et al. (2022) and this study, Fürst et al. (2018) locally calibrated their method against point thickness observations, implying low errors close to observation sites. Based on this, we excluded Fürst et al. (2018) from the thickness comparison in Table 2. In general, our study shows more similarities in terms of spatial distribution with Fürst et al. (2018) than with Millan et al. (2022). The inverse method in Millan et al. (2022) relies on ice velocities and inversion of the SIA, with a parameterized description of sliding, to estimate thickness. The overestimation of ice thickness for large glaciers in Millan et al. (2022) (Table 2), and most prominently for surging glaciers, e.g. Basin-3, Tunabreen, Negribreen and Storebreen (Fig. 8) could result from inappropriate physics to describe the highly dynamic and complex flow. The same argument, in addition to mismatches in the timing of input datasets, has led us to use the simpler perfect-plasticity method for surging glaciers in this study. Finally, in comparison with Fürst et al. (2018), both our study and Millan et al. (2022) find thicker ice in most low-elevation valleys of both small and larger glaciers. For the large Austfonna ice cap, our study and Fürst et al. (2018) are in better agreement than our study and Millan et al. (2022); most notably our study and Fürst et al. (2018) experience less pronounced jumps near ice divides.

4.3 Uncertainties

By applying dedicated inverse methods and model physics for different glacier types, using state-of-the-art remote sensing and model input datasets, and calibrating against thickness observations, we limit uncertainties in the final thickness and bed maps. As noted before, in the hypothetical case of perfectly accurate ice flow physics, and flawless and synchronous input datasets (climatic mass balance, surface height, surface height change and surface velocity), an error-free bed map (except for fine-scale topography) can be generated with iterative updates of basal boundary conditions (bed height and friction) in an ice flow model. Although this is fictitious, it does give directions for future improvement of inverse estimation of basal conditions, which among others demands a better description of ice flow physics, and higher quality and synchronous input and validation datasets. For a more extensive discussion on thickness error sources, e.g. from inaccurate model physics, inverse model parameters, and noisy input datasets, we refer to Frank et al. (2023) and Frank and Van Pelt (2024).

The validation of local ice thicknesses against available observations (Sect. 4.2) gives a direct estimate of the uncertainty of bed heights and thicknesses for these locations. Instead, the total volume uncertainty cannot be directly quantified and is here based on the assumption that it is the sum of errors resulting from uncertainty in glacier extent (extracted from the RGI database) and modeled mean thickness. Our statistical method to estimate uncertainty in mean ice thickness (Sect. 3.5) captures

https://doi.org/10.5194/egusphere-2024-1525
Preprint. Discussion started: 31 May 2024

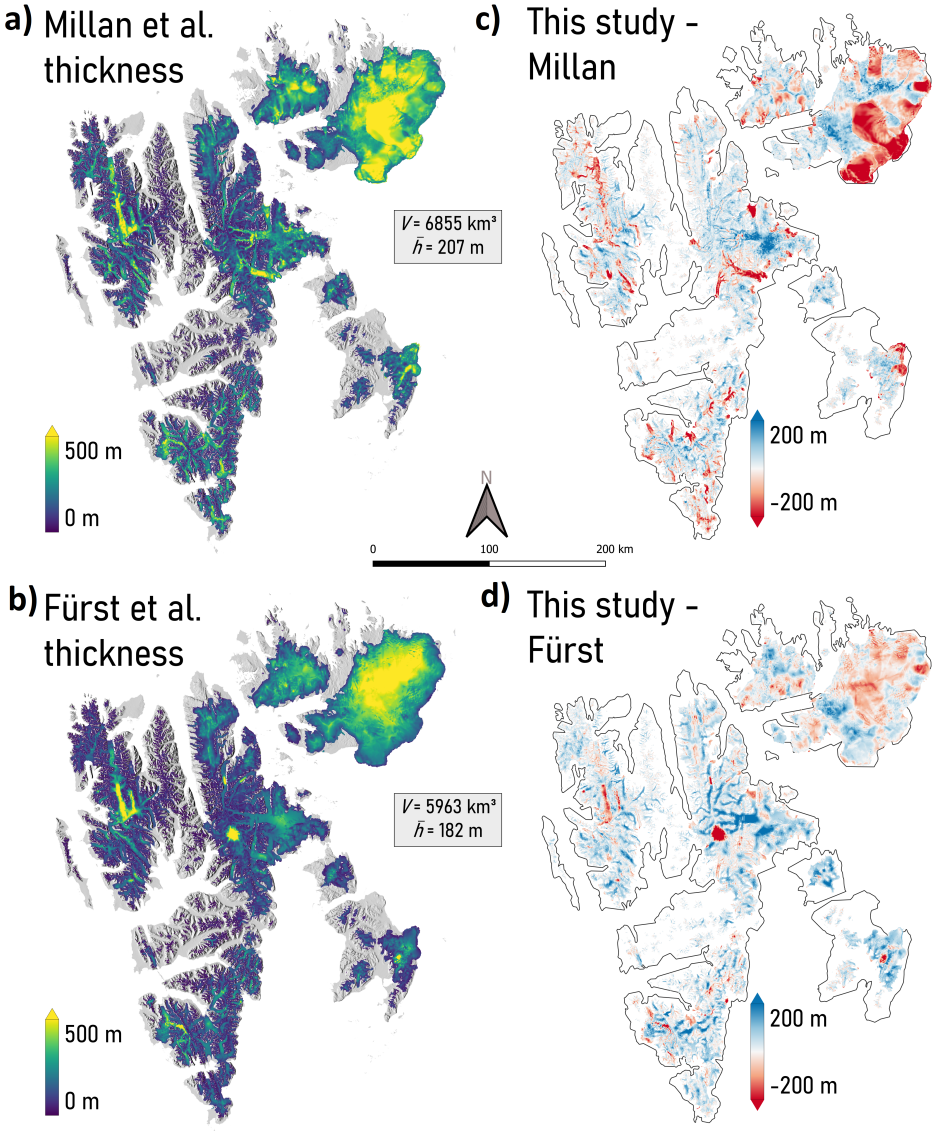

Figure 8. Previous ice thickness maps by Millan et al. (2022) (a) and Fürst et al. (2018) (b), and the corresponding differences with our results (c-d).

all errors that may result from the fact that thickness observations against which the models are calibrated may be spatially biased (e.g. when a certain glacier type or region is over-represented). The large and well-distributed thickness observations dataset available for Svalbard hence helps to reduce the volume uncertainty. The real volume uncertainty could be larger than anticipated in case the uncertainty of glacier extent in the RGI outlines for Svalbard is larger than the 1-2% that Nuth et al. (2013) estimated. Furthermore, systematic observational biases in thickness observations (e.g. instrumental or data processing

https://doi.org/10.5194/egusphere-2024-1525
Preprint. Discussion started: 31 May 2024

errors such as radar travel time to thickness conversions) may create additional volume uncertainty, although there are no indications for this.

Given the different (average) timings of input datasets, it is hard to set a date for what point in time the bed and thickness maps represent, but a rough best estimate would be 2010-2015, which is the median for key input datasets of surface height, surface height change, ice velocity, climatic mass balance, and glacier outlines. Ice thickness observations in GlaThiDa have been collected from 1983 to 2016, and represent a mean date (∼year 2009-2010) that is three years earlier than the representative date of the model output. With previously estimated thinning in Svalbard of ∼-0.35 m per year in 1936-2010 (Geyman et al., 2022), i.e. 0.17% relative volume loss per year, the real volume in 2010-2015 may have been ∼35 km^3 smaller than we modeled. Similarly, a retreat of glaciers of -39 km^2 per year (1936-2010; Geyman et al., 2022), or a relative area loss of 0.12% per year, implies an additional potential volume loss of -39 km^3 between the mean collection date of glacier outlines (2007-2008) and the reference time for our thickness map. These volume bias estimates should be regarded as rough estimates, e.g. as the actual rates of area and thickness change may have differed from the used 1936-2010 averages. Finally, the different timing of input datasets complicates the inversion of thickness for glaciers that experience rapid geometric and dynamic changes. This particularly applies to surging glaciers, where the application of iterative inverse methods would introduce excessive errors primarily due to timing mismatches between surface height, surface height change, and velocity datasets. In case such timing mismatches can be reduced, we would recommend the use of iterative inverse methods also for surging glaciers in future experiments. Nevertheless, thickness inversion for surging glaciers would likely still be less accurate than for other glaciers because of the lack of appropriate ice flow physics in commonly used ice flow models.

5 Conclusions

We present a new bed height and thickness map for all glaciers in Svalbard, generated using a combination of three inverse methods. Combining the methods allows us to simulate small land-terminating glaciers with high spatial resolution (100-m) using the deep-learning model IGM, whereas thickness inversion for large tidewater and land-terminating glaciers benefits from a SIA+SSA approach in PISM to describe sliding motion. Input data uncertainty for actively surging glaciers led us to use a simple perfect-plasticity-based method for those glaciers. Comparison of thicknesses with observations reveals good agreement with point observations for glaciers of different types. Particularly, for large and tidewater glaciers we find improved estimates of ice thickness compared to a previous study by Millan et al. (2022). We find that Svalbard's glaciers, excluding Kvitøya, have a volume of 6,800±238 km^3 (16.3±0.6 mm sea-level equivalent) and a mean thickness of 205±7 m, which is in between recent estimates of 5,963 km^3 or 182 m (Fürst et al., 2018) and 6,855 km^3 or 207 m (Millan et al., 2022), generated using entirely independent methodologies.

The bed and thickness datasets are made available in open-access databases and may find further applications within glaciology and other fields (e.g. in studies of runoff and impacts on fjord processes). A benefit of the thickness map produced with iterative inverse methods, i.e. for all not actively surging glaciers, is that it simultaneously provides initial conditions for future simulation of Svalbard's glaciers.

https://doi.org/10.5194/egusphere-2024-1525
Preprint. Discussion started: 31 May 2024

Code and data availability. The bed and thickness datasets, presented in Fig. 3, together with the mask shown in Fig. 1c, are uploaded as Geotiff-files to the following repository: https://doi.org/10.5281/zenodo.11239460. The source code of the Parallel Ice Sheet Model can be accessed at https://www.pism.io/. The Instructed Glacier Model is available at https://github.com/jouvetg/igm.

Author contributions. Both authors (WvP and TF) contributed substantially to the study design, the modelling experiments, data analysis and manuscript writing.

Competing interests. There are no competing interests.

Acknowledgements. WvP acknowledges funding from a career grant by the Swedish National Space Agency (2018-C; project nr. 189/18) and a starting grant by the Swedish Research Council (project nr. 2020-04319). Development of PISM is supported by NASA grants 20-CRYO2020-0052 and 80NSSC22K0274 and NSF grant OAC-2118285.

https://doi.org/10.5194/egusphere-2024-1525
Preprint. Discussion started: 31 May 2024

References

Bintanja, R. and Van der Linden, E. C.: The changing seasonal climate in the Arctic, Scientific Reports, https://doi.org/10.1038/srep01556, 2013.

Bochow, N., Poltronieri, A., Robinson, A., Montoya, M., Rypdal, M., and Boers, N.: Overshooting the critical threshold for the Greenland ice sheet, Nature, 622, 528–536, https://doi.org/10.1038/s41586-023-06503-9, 2023.

Bueler, E. and Brown, J.: Shallow shelf approximation as a "sliding law" in a thermomechanically coupled ice sheet model, Journal of Geophysical Research: Earth Surface, 114, https://doi.org/10.1029/2008jf001179, 2009.

Cao, Y., Liang, S., Chen, X., He, T., Wang, D., and Cheng, X.: Enhanced wintertime greenhouse effect reinforcing Arctic amplification and initial sea-ice melting, Scientific Reports, 7, https://doi.org/10.1038/s41598-017-08545-2, 2017.

Cook, S. J., Jouvet, G., Millan, R., Rabatel, A., Zekollari, H., and Dussaillant, I.: Committed Ice Loss in the European Alps Until 2050 Using a Deep-Learning-Aided 3D Ice-Flow Model With Data Assimilation, Geophysical Research Letters, 50, https://doi.org/10.1029/2023gl105029, 2023.

Farinotti, D., Huss, M., Bauder, A., Funk, M., and Truffer, M.: A method to estimate the ice volume and ice-thickness distribution of alpine glaciers, Journal of Glaciology, 55, 422–430, https://doi.org/10.3189/002214309788816759, 2009.

Farinotti, D., Brinkerhoff, D. J., Clarke, G. K. C., Fürst, J. J., Frey, H., Gantayat, P., Gillet-Chaulet, F., Girard, C., Huss, M., Leclercq, P. W., Linsbauer, A., Machguth, H., Martin, C., Maussion, F., Morlighem, M., Mosbeux, C., Pandit, A., Portmann, A., Rabatel, A., Ramsankaran, R., Reerink, T. J., Sanchez, O., Stentoft, P. A., Singh Kumari, S., van Pelt, W. J. J., Anderson, B., Benham, T., Binder, D., Dowdeswell, J. A., Fischer, A., Helfricht, K., Kutuzov, S., Lavrentiev, I., McNabb, R., Gudmundsson, G. H., Li, H., and Andreassen, L. M.: How accurate are estimates of glacier ice thickness? Results from ITMIX, the Ice Thickness Models Intercomparison eXperiment, The Cryosphere, 11, 949–970, https://doi.org/10.5194/tc-11-949-2017, 2017.

Farinotti, D., Huss, M., Fürst, J. J., Landmann, J., Machguth, H., Maussion, F., and Pandit, A.: A consensus estimate for the ice thickness distribution of all glaciers on Earth, Nature Geoscience, 12, 168–173, https://doi.org/10.1038/s41561-019-0300-3, 2019.

Farinotti, D., Brinkerhoff, D. J., Fürst, J. J., Gantayat, P., Gillet-Chaulet, F., Huss, M., Leclercq, P. W., Maurer, H., Morlighem, M., Pandit, A., Rabatel, A., Ramsankaran, R., Reerink, T. J., Robo, E., Rouges, E., Tamre, E., van Pelt, W. J. J., Werder, M. A., Azam, M. F., Li, H., and Andreassen, L. M.: Results from the Ice Thickness Models Intercomparison eXperiment Phase 2 (ITMIX2), Frontiers in Earth Science, 8, https://doi.org/10.3389/feart.2020.571923, 2021.

Frank, T. and Van Pelt, W. J. J.: Ice volume and thickness of all Scandinavian glaciers and ice caps, Journal of Glaciology, pp. 1–14, https://doi.org/10.1017/jog.2024.25, 2024.

Frank, T., Van Pelt, W. J. J., and Kohler, J.: Reconciling ice dynamics and bed topography with a versatile and fast ice thickness inversion, The Cryosphere, 17, 4021–4045, https://doi.org/10.5194/tc-17-4021-2023, 2023.

Fürst, J. J., Gillet-Chaulet, F., Benham, T. J., Dowdeswell, J. A., Grabiec, M., Navarro, F., Pettersson, R., Moholdt, G., Nuth, C., Sass, B., Aas, K., Fettweis, X., Lang, C., Seehaus, T., and Braun, M.: Application of a two-step approach for mapping ice thickness to various glacier types on Svalbard, The Cryosphere, 11, 2003–2032, https://doi.org/10.5194/tc-11-2003-2017, 2017.

Fürst, J. J., Navarro, F., Gillet-Chaulet, F., Huss, M., Moholdt, G., Fettweis, X., Lang, C., Seehaus, T., Ai, S., Benham, T. J., Benn, D. I., Björnsson, H., Dowdeswell, J. A., Grabiec, M., Kohler, J., Lavrentiev, I., Lindbäck, K., Melvold, K., Pettersson, R., Rippin, D., Saintenoy, A., Sánchez-Gámez, P., Schuler, T. V., Sevestre, H., Vasilenko, E., and Braun, M. H.: The Ice-Free Topography of Svalbard, Geophysical Research Letters, 45, 11,760–11,769, https://doi.org/10.1029/2018gl079734, 2018.

https://doi.org/10.5194/egusphere-2024-1525
Preprint. Discussion started: 31 May 2024

Geyman, E. C., J. J. van Pelt, W., Maloof, A. C., Aas, H. F., and Kohler, J.: Historical glacier change on Svalbard predicts doubling of mass loss by 2100, Nature, 601, 374–379, https://doi.org/10.1038/s41586-021-04314-4, 2022.

GlaThiDa Consortium: Glacier Thickness Database (GlaThiDa), World Glacier Monitoring Service (WGMS), https://doi.org/10.5904/WGMS-GLATHIDA-2020-10, 2020.

Goelzer, H., Robinson, A., Seroussi, H., and van de Wal, R. S.: Recent Progress in Greenland Ice Sheet Modelling, Current Climate Change Reports, 3, 291–302, https://doi.org/10.1007/s40641-017-0073-y, 2017.

Grinsted, A.: An estimate of global glacier volume, The Cryosphere, 7, 141–151, https://doi.org/10.5194/tc-7-141-2013, 2013.

Gudmundsson, G. H. and Raymond, M.: On the limit to resolution and information on basal properties obtainable from surface data on ice streams, The Cryosphere, 2, 167–178, https://doi.org/10.5194/tc-2-167-2008, 2008.

Gärtner-Roer, I., Naegeli, K., Huss, M., Knecht, T., Machguth, H., and Zemp, M.: A database of worldwide glacier thickness observations, Global and Planetary Change, 122, 330–344, https://doi.org/10.1016/j.gloplacha.2014.09.003, 2014.

Hagen, J. O., ed.: Glacier atlas of Svalbard and Jan Mayen, no. 129 in Meddelelser, Nork Polarinstitutt, Oslo, 1993.

Hugonnet, R., McNabb, R., Berthier, E., Menounos, B., Nuth, C., Girod, L., Farinotti, D., Huss, M., Dussaillant, I., Brun, F., and Kääb, A.: Accelerated global glacier mass loss in the early twenty-first century, Nature, 592, 726–731, https://doi.org/10.1038/s41586-021-03436-z, 2021.

IPCC: Climate Change 2023: Synthesis Report. Contribution of Working Groups I, II and III to the Sixth Assessment Report of the Intergovernmental Panel on Climate Change [Core Writing Team, H. Lee and J. Romero (eds.)]. IPCC, Geneva, Switzerland., https://doi.org/10.59327/ipcc/ar6-9789291691647, 2023.

Jouvet, G.: Inversion of a Stokes glacier flow model emulated by deep learning, Journal of Glaciology, 69, 13–26, https://doi.org/10.1017/jog.2022.41, 2022.

Jouvet, G. and Cordonnier, G.: Ice-flow model emulator based on physics-informed deep learning, Journal of Glaciology, pp. 1–15, https://doi.org/10.1017/jog.2023.73, 2023.

Koch, M., Seehaus, T., Friedl, P., and Braun, M.: Automated Detection of Glacier Surges from Sentinel-1 Surface Velocity Time Series—An Example from Svalbard, Remote Sensing, 15, 1545, https://doi.org/10.3390/rs15061545, 2023.

Kochtitzky, W., Copland, L., Van Wychen, W., Hugonnet, R., Hock, R., Dowdeswell, J. A., Benham, T., Strozzi, T., Glazovsky, A., Lavrentiev, I., Rounce, D. R., Millan, R., Cook, A., Dalton, A., Jiskoot, H., Cooley, J., Jania, J., and Navarro, F.: The unquantified mass loss of Northern Hemisphere marine-terminating glaciers from 2000–2020, Nature Communications, 13, https://doi.org/10.1038/s41467-022-33231-x, 2022.

Li, H., Ng, F., Li, Z., Qin, D., and Cheng, G.: An extended "perfect-plasticity" method for estimating ice thickness along the flow line of mountain glaciers, Journal of Geophysical Research: Earth Surface, 117, https://doi.org/10.1029/2011jf002104, 2012.

Linsbauer, A., Paul, F., Hoelzle, M., Frey, H., and Haeberli, W.: The Swiss Alps without glaciers – a GIS-based modelling approach for reconstruction of glacier beds, https://doi.org/10.5167/UZH-27834, 2009.

Martin, M. A., Winkelmann, R., Haseloff, M., Albrecht, T., Bueler, E., Khroulev, C., and Levermann, A.: The Potsdam Parallel Ice Sheet Model (PISM-PIK) – Part 2: Dynamic equilibrium simulation of the Antarctic ice sheet, The Cryosphere, 5, 727–740, https://doi.org/10.5194/tc-5-727-2011, 2011.

Martín-Español, A., Navarro, F., Otero, J., Lapazaran, J., and Błaszczyk, M.: Estimate of the total volume of Svalbard glaciers, and their potential contribution to sea-level rise, using new regionally based scaling relationships, Journal of Glaciology, 61, 29–41, https://doi.org/10.3189/2015jog14j159, 2015.

https://doi.org/10.5194/egusphere-2024-1525
Preprint. Discussion started: 31 May 2024

Millan, R., Mouginot, J., Rabatel, A., and Morlighem, M.: Ice velocity and thickness of the world's glaciers, Nature Geoscience, 15, 124–129, https://doi.org/10.1038/s41561-021-00885-z, 2022.

Morlighem, M.: IceBridge BedMachine Greenland, Version 5, https://doi.org/10.5067/GMEVBWFLWA7X, 2022.

Norwegian Polar Institute: Terrengmodell Svalbard (S0 Terrengmodell) [Data set]. Norwegian Polar Institute, https://doi.org/10.21334/npolar.2014.dce53a47, 2014.

Noël, B., Jakobs, C. L., van Pelt, W. J. J., Lhermitte, S., Wouters, B., Kohler, J., Hagen, J. O., Luks, B., Reijmer, C. H., van de Berg, W. J., and van den Broeke, M. R.: Low elevation of Svalbard glaciers drives high mass loss variability, Nature Communications, 11, https://doi.org/10.1038/s41467-020-18356-1, 2020.

Nuth, C., Kohler, J., König, M., Deschwanden, A. V., Hagen, J. O., Kääb, A., Moholdt, G., and Pettersson, R.: Decadal changes from a multi-temporal glacier inventory of Svalbard, Cryosphere, https://doi.org/10.5194/tc-7-1603-2013, 2013.

Nye, J. F.: The Mechanics of Glacier Flow, Journal of Glaciology, 2, 82–93, https://doi.org/10.3189/s0022143000033967, 1952.

Ohmura, A.: Cryosphere during the twentieth century, pp. 239–257, American Geophysical Union, https://doi.org/10.1029/150gm19, 2004.

Radić, V. and Hock, R.: Regional and global volumes of glaciers derived from statistical upscaling of glacier inventory data, Journal of Geophysical Research: Earth Surface, 115, https://doi.org/10.1029/2009jf001373, 2010.

Radić, V. and Hock, R.: Glaciers in the Earth's Hydrological Cycle: Assessments of Glacier Mass and Runoff Changes on Global and Regional Scales, pp. 813–837, Springer Netherlands, https://doi.org/10.1007/978-94-017-8789-5_15, 2013.

RGI Consortium: Randolph Glacier Inventory - A Dataset of Global Glacier Outlines, Version 6, National Snow and Ice Data Center, https://doi.org/10.7265/4M1F-GD79, 2017.

Robinson, R.: Modeling the Flow Dynamics of the Langjökull Ice Cap, Iceland, Master's thesis, University of Iceland, 2018.

Rounce, D. R., Hock, R., Maussion, F., Hugonnet, R., Kochtitzky, W., Huss, M., Berthier, E., Brinkerhoff, D., Compagno, L., Copland, L., Farinotti, D., Menounos, B., and McNabb, R. W.: Global glacier change in the 21st century: Every increase in temperature matters, Science, 379, 78–83, https://doi.org/10.1126/science.abo1324, 2023.

Schuler, T. V., Kohler, J., Elagina, N., Hagen, J. O. M., Hodson, A. J., Jania, J. A., Kääb, A. M., Luks, B., Małecki, J., Moholdt, G., Pohjola, V. A., Sobota, I., and Van Pelt, W. J. J.: Reconciling Svalbard Glacier Mass Balance, Frontiers in Earth Science, 8, https://doi.org/10.3389/feart.2020.00156, https://www.frontiersin.org/article/10.3389/feart.2020.00156/full, 2020.

Serreze, M. C. and Barry, R. G.: Processes and impacts of Arctic amplification: A research synthesis, Global and Planetary Change, https://doi.org/10.1016/j.gloplacha.2011.03.004, 2011.

Sevestre, H. and Benn, D. I.: Climatic and geometric controls on the global distribution of surge-type glaciers: implications for a unifying model of surging, Journal of Glaciology, 61, 646–662, https://doi.org/10.3189/2015jog14j136, 2015.

Van Pelt, W., Pohjola, V., Pettersson, R., Marchenko, S., Kohler, J., Luks, B., Hagen, J. O., Schuler, T. V., Dunse, T., Noël, B., and Reijmer, C.: A long-term dataset of climatic mass balance, snow conditions, and runoff in Svalbard (1957–2018), The Cryosphere, 13, 2259–2280, https://doi.org/10.5194/tc-13-2259-2019, https://tc.copernicus.org/articles/13/2259/2019/, 2019.

Van Pelt, W. J. J., Oerlemans, J., Reijmer, C. H., Pettersson, R., Pohjola, V. A., Isaksson, E., and Divine, D.: An iterative inverse method to estimate basal topography and initialize ice flow models, The Cryosphere, 7, 987–1006, https://doi.org/10.5194/tc-7-987-2013, 2013.

Van Pelt, W. J. J., Schuler, T. V., Pohjola, V. A., and Pettersson, R.: Accelerating future mass loss of Svalbard glaciers from a multi-model ensemble, Journal of Glaciology, 67, 485–499, https://doi.org/10.1017/jog.2021.2, 2021.